13. Extreme care was taken to ensure that there were no impurities in the beam that might oxidize the surface.

14. M. H. Matloob and M. W. Roberts, *Phys. Scr.* **16**, 420 (1977).

15. The mechanism of oxidation is thought to be dissociative adsorption of NO. The removal of nitrogen adatoms may be explained in several ways: (i) reaction of adsorbed N atoms with NO in the molecular beam to form N_2O (which desorbs), (ii) the selective recombination of nitrogen adatoms to form desorbing N_2, or (iii) the reaction of two adsorbed NO molecules to form N_2O (which desorbs) + O, which is known to be important at low surface temperatures when the NO coverage is high.

16. The ratio of AES signals for Cu and O on this surface revealed a ratio of O adatom to surface Cu atom of ~1:3. This relied on a calibration of the AES response [F. H. P. M. Habraken, E. P. Kieffer, G. A. Bootsma, *Surf. Sci.* **83**, 45 (1979)].

17. M. Drabbels and A. M. Wodtke, *J. Chem. Phys.* **106**, 3024 (1997).

18. One photon excited the NO resonantly to the $A^2\Sigma^+$ state and a second photon ionized the molecules in the $A^2\Sigma^+$ state. For the experiments reported here, neither step of the REMPI process was saturated.

19. H. Hou *et al.*, *J. Chem. Phys.*, in press.

20. A significant background signal due to population of NO ($v = 13$) by the pump laser alone (known as Franck-Condon pumping background) has already been subtracted. This is done by analyzing the scattered REMPI signal with and without the dump laser. Because the dump transition induces a large fractional decrease in the population of the excited electronic level, $\delta n_{ex}/n_{ex}$ (~0.15), the net scattering signal is given as $S_{net} = S_3 - S_2[1 - (\delta n_{ex}/n_{ex})]$, where S_2 and S_3 are the two- and three-laser signals, respectively. $\delta n_{ex}/n_{ex}$ was measured from fluorescence dips. For analysis and display in Fig. 3, S_{net} was normalized to the square of the probe laser power.

21. After absolute wavelength calibration of the spectrum, the data shown here were fit using intermediate-case Hönl-London factors [R. N. Zare, *Angular Momentum* (Wiley-Interscience, New York, 1987), p. 314; note that the first P_2 branch in the table is actually the P_{21} branch]. Energy levels of the ground state are from C. Amiot, *J. Mol. Spectrosc.* **94**, 150 (1982). Energy levels for the A state derive from R. Engleman Jr., P. E. Rouse, H. M. Peek, V. D. Baiamonte, *Los Alamos Science Lab Report LA-4364* (1970); R. Engleman Jr. and P. E. Rouse, *J. Mol. Spectrosc.* **37**, 240 (1971). The rotational state populations were modeled by a Boltzmann distribution.

22. Here, one ML indicates 1.6×10^{15} molecules cm^{-2}.

23. The following channels were observed ($v = 15 \rightarrow 13$, $15 \rightarrow 10$, $13 \rightarrow 12$, $13 \rightarrow 10$, $13 \rightarrow 9$, $12 \rightarrow 9$).

24. Because of the difficulty of ensuring an absolutely oxygen-free surface and the high sensitivity of the REMPI signal to oxygen coverage, we consider this number to be a lower limit to the true value. The error bars represent one standard deviation.

25. Temperatures between 300 and 500 K were studied. Two molecular beams were compared with collision energies of 29 and 67 kJ/mol.

26. C. T. Rettner, D. J. Auerbach, J. C. Tully, A. W. Kleyn, *J. Phys. Chem.* **100**, 13021 (1996).

27. J. C. Polanyi, *Acc. Chem. Res.* **5**, 161 (1972); _____ and W. H. Wong, *J. Chem. Phys.* **51**, 1439 (1969).

28. Supported by the U.S. Air Force Office of Scientific Research (grant F49620-95-1-0234) and the U.S. Department of Energy Office of Basic Energy Sciences (grant DE-FG03-94ER14492/A000).

7 January 1999; accepted 5 May 1999

Adsorbed Layers and the Origin of Static Friction

Gang He, Martin H. Müser,* Mark O. Robbins†

Analytic results and experiments in ultrahigh vacuum indicate that the static friction between two clean crystalline surfaces should almost always vanish, yet macroscopic objects always exhibit static friction. A simple and general explanation for the prevalence of static friction is proposed. "Third bodies," such as small hydrocarbon molecules, adsorb on any surface exposed to air and can arrange to lock two contacting surfaces together. The resulting static friction is consistent with experimental behavior, including Amontons' laws.

Amontons' laws, which are 300 years old, state that the frictional force F needed to slide one body laterally over another is independent of their macroscopic area of contact and proportional to the normal load L that presses them together (*1, 2*). The constant of proportionality $\mu = F/L$, or coefficient of friction, depends on the materials and whether the bodies are at rest (μ_s) or in motion (μ_k).

Despite the success of Amontons' laws, there is no microscopic theory that explains their molecular origins and wide-ranging applicability. In fact, analytic theories indicate that static friction, the force F_s needed to initiate motion between two bodies at rest, should vanish between almost any pair of clean surfaces that deform elastically (*3–6*). These theories, and many simulation studies, only include atoms in the two bodies that move past each other. However, there is almost always some form of "third body" present between two surfaces. Indeed, Amon-

tons measured static friction for greased surfaces (*1*), and any surface exposed to ambient air acquires an adsorbed layer of hydrocarbons and other small molecules that is a few angstroms thick. Larger particles may also be present in the form of dust or wear debris.

We report molecular dynamics simulations that show that third bodies naturally lead to a nonzero static friction. Moreover, the static friction produced by adsorbed layers of short molecules is consistent with Amontons' laws and does not vary substantially with parameters that are usually not controlled in experiments, such as the precise thickness and chemistry of adsorbed layers, the orientational alignment of surfaces, and the direction of sliding relative to crystalline axes.

The actual area of molecular contact between two surfaces, A_{real}, is generally the small fraction of the apparent macroscopic area where peaks on opposing surfaces meet (*2, 7, 8*). Elastic deformation flattens the contact regions into micrometer diameter patches, orders of magnitude larger than individual molecules. The static friction corresponds to an average yield stress within these contacts of $\tau_s = F_s/A_{real}$.

Bowden and Tabor suggested a simple phenomenological form for τ_s that explains the

successes of Amontons' laws and some of their failures (*2*). If the yield stress rises linearly with the local pressure $P = L/A_{real}$, then

$$\tau_s = \tau_0 + \alpha P \qquad (1)$$

One finds $F_s = \tau_0 A_{real} + \alpha L$ or

$$\mu_s = \alpha + \tau_0/P \qquad (2)$$

Thus, μ_s is independent of load and macroscopic area if P is constant or if P is much greater than τ_0. The former applies to simple models of ideally elastic (*9*) and plastic surfaces (*2*). Amontons' laws are known to fail when P varies substantially or τ_0 is large (strong adhesion), but Eqs. 1 and 2 remain valid (*10–13*).

The theoretical difficulty is that a nonzero τ_s requires that the surfaces lock together in a local free-energy minimum that prevents sliding (*3–6*). Every atom on two identical aligned crystals (Fig. 1A) can simultaneously lie at a local energy minimum and contribute coherently to τ_s. When the surfaces are rotated by almost any angle (Fig. 1, B and C) or have different lattice constants (Fig. 1D), the number of atoms resisting lateral motion is exactly equaled by the number assisting it. Such incommensurate surfaces have no static friction unless the interaction between them is so strong, compared to the interactions within the solids, that the surface atoms rearrange to create a local energy minimum (*3, 4, 14, 15*). Experimental studies of friction between clean crystalline surfaces are limited (*16*) but are consistent with this conclusion. Krim and co-workers measured no static friction between substrates and incommensurate adsorbed layers (*17*), and their data are consistent with simulations (*18*). Small crystalline atomic force microscope (AFM) tips show substantial static friction only at commensurate alignments (*19*). Finally, the friction between unaligned MoS_2 crystals is extremely low in ultrahigh vacuum but rises rapidly with exposure to air (*20*).

Third bodies such as airborne hydrocarbons

Department of Physics and Astronomy, Johns Hopkins University, Baltimore, MD 21218, USA.

*Present address: Institut für Physik, WA 331, Johannes Gutenberg-Universität, 55099 Mainz, Germany.
†To whom correspondence should be addressed: E-mail: mr@pha.jhu.edu

are free to move along the interface to produce a local energy minimum without deforming the solids that confine them. Previous simulations demonstrate the importance of third bodies to both static and kinetic friction but have been limited to commensurate surfaces (21–25). Controlled experiments on hydrocarbons between mica and other molecularly smooth surfaces show that thicknesses of a few molecular layers or less result in a static friction that satisfies Eq. 1 (12, 13). However, these experiments only access pressures on the order of 30 MPa. In order for adsorbed layers to explain experimental observations in typical macroscopic contacts, they must obey Eq. 1 up to gigapascal pressures with reasonable values of τ_0 and α. Moreover, the value of α should depend on the chemical constituents of the two surfaces but not on parameters that are not controlled in experiments. As we now show, adsorbed layers meet these requirements.

We simulated the adsorbed molecules with a simple bead-spring model (26) that has successfully reproduced the behavior of confined hydrocarbon films (23). Each adsorbed molecule contains n spherical monomers that are bound to make a linear chain. All monomers interact with a truncated Lennard-Jones potential $V^{\mathrm{LJ}}(r) = 4\varepsilon[(\sigma/r)^{12}-(\sigma/r)^6]$ for separations $r < r_{\mathrm{c}}$, where ε and σ are characteristic energy and length scales, respectively. Adjacent monomers on a chain are bound by a potential $V^{\mathrm{CH}}(r) = -(1/2)kR_{\mathrm{o}}^2\ln[1 - (r/R_{\mathrm{o}})^2]$, where $R_{\mathrm{o}} = 1.5\sigma$ and $k = 30\varepsilon/\sigma^2$. The results presented below are expressed in terms of ε, σ, and $t_0 \equiv \sqrt{m\sigma^2/\varepsilon}$, where m is the monomer mass. Values that would be representative of hydrocarbons are as follows (26): $\varepsilon \sim 30$ meV, $\sigma \sim 0.5$ nm, and $t_0 \sim 3$ ps. The unit of pressure is $\varepsilon\sigma^{-3} \sim 40$ MPa. Short-chain hydrocarbons are liquids at room temperature, so we show results for temperature $T = 0.7\varepsilon/k_{\mathrm{B}}$ (where k_{B} is Boltzmann's constant). Runs at other temperatures produced similar results.

The monomers were confined between walls composed of discrete atoms. Although the detailed dissipation mechanisms that produce kinetic friction might be sensitive to the interactions between wall atoms, the static friction depends mainly on the geometry and

compliance of the walls. We considered the extreme case of stiff walls to demonstrate that adsorbed monomers could change the static friction from zero to a finite value. Wall atoms interacted with adsorbed monomers through a Lennard-Jones potential with energy and length scales ε_{w} and σ_{w}, respectively. The atoms were tied to sites with springs of stiffness κ, and the sites were arranged to form a crystal or amorphous solid.

We found similar behavior for a wide range of wall geometries and will focus here on those shown in Fig. 1. Here, atoms are on (111) surfaces of face-centered cubic crystals with nearest neighbor spacing d on the bottom surface. In Fig. 1, A through C, two identical surfaces are rotated by different angles relative to each other, and in Fig. 1D, the surfaces have slightly different lattice constants. Because we are interested in calculating the yield stress of a small portion of a micrometer-size contact, we imposed periodic boundary conditions in the plane of the walls. This makes it impossible to have strictly incommensurate walls, but we verified that the boundary conditions have little effect on the yield stress by studying system size dependence. We also verified that there was no static friction between the "incommensurate" walls for any reasonable value of κ when the adsorbed layer was absent. Except where noted, we show data for $n = 6$, $\kappa = \infty$, $\varepsilon_{\mathrm{w}} = \varepsilon$, $\sigma_{\mathrm{w}} = \sigma$, $r_{\mathrm{c}} = 2^{1/6}\sigma$, and $d = 1.2\sigma$.

The static friction for each system and pressure was determined by ramping or stepping the force until the system began to slide. The yield stress τ_{s} was insensitive to the rate at which the force was changed. Figure 2A compares τ_{s} for the different surfaces shown in Fig. 1 at an adsorbate coverage of 1/8, which is defined as the ratio of monomers to wall atoms on each surface before they are brought into contact. Each set of data falls onto the straight line implied by Eq. 1 up to $P = 36\varepsilon\sigma^{-3}$ or ~ 1.5 GPa. The incommensurate cases (Fig. 1, B through D) give the same $\alpha = 0.048 \pm 0.02$. The values of τ_0 are small, and the differences in them are comparable to statistical fluctuations in the data. The same friction is also found for sliding along inequivalent lattice directions,

for example, along x and y in Fig. 1D (Fig. 2A, up and down triangles). Only the commensurate case (Fig. 2A, circles) produces different values of F_{s}. As expected, the friction is higher ($\alpha = 0.15$) because of the uniform registry between the two surfaces. However, the ratio between commensurate and incommensurate values of α has been reduced from infinity to a factor of 3 because of the presence of an adsorbed layer.

We have considered many other parameter sets to determine which factors influence α and τ_0. Decreasing κ to make the surfaces more compliant would increase the ability of bare surfaces to lock together but actually decreases τ_{s} slightly when adsorbed layers are present. The extra compliance makes it easier for wall atoms to move out of the way and allow sliding to start. The alignment of the surfaces and the direction of sliding always leave τ_{s} nearly unchanged, except in the unlikely case of commensurate surfaces. Other parameters that are not controlled in experiments have little effect on μ_{s}. For example, decreasing the chain length n from 6 to 3 to 1 for the parameters of Fig. 2A produces no noticeable change in τ_{s}. There are small changes in τ_0 with coverage, but these are only important at low pressures. Increasing the coverage on each surface up to one or more monolayers on separated surfaces produces little change in the value of α ($\sim 10\%$ over coverages from 1/4 to 1). Previous studies of adsorbed layers between commensurate surfaces found little variation in kinetic friction with
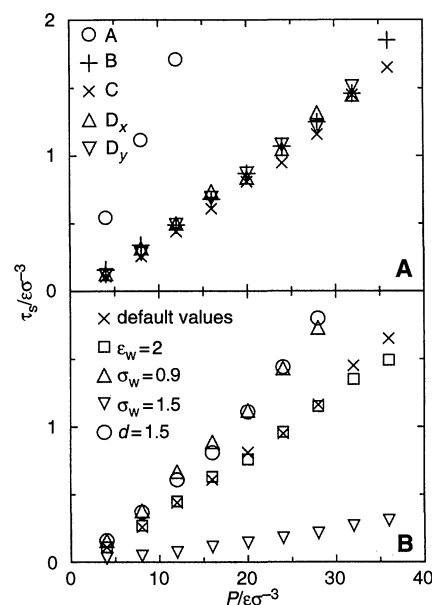
Fig. 2. Yield stress τ_{s} versus pressure P. Statistical errors are less than or equal to the symbol size, and $\varepsilon\sigma^{-3} \sim 40$ MPa. **(A)** Results for the different walls shown in Fig. 1 at a coverage of 1/8. Results for two inequivalent sliding directions, x and y, are shown for system D. **(B)** Results for different potential parameters. Default values are $n = 6$, $\kappa = \infty$, $\varepsilon_{\mathrm{w}} = \varepsilon$, $\sigma_{\mathrm{w}} = \sigma$, $r_{\mathrm{c}} = 2^{1/6}\sigma$, and $d = 1.2\sigma$.
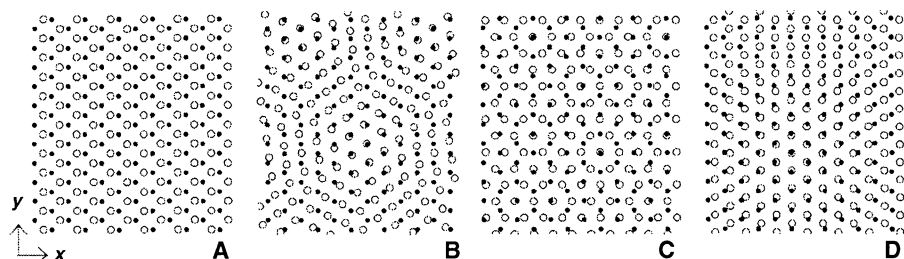
Fig. 1. Projections of atoms from the bottom (solid circles) and top (open circles) surfaces into the plane of the walls. **(A through C)** The two walls have the same structure and lattice constant, but the top wall has been rotated by 0°, 11.6°, or 90°, respectively. **(D)** The walls are aligned, but the lattice constant of the top wall has been reduced by 12/13. The atoms can only achieve perfect registry in the commensurate case (A). The simulation cell was at least four times the area shown here.

chain length or coverage (24).

The value of τ_0 represents the adhesive contribution to friction because it gives the yield stress in the absence of an external pressure. In Fig. 2A, the interactions are purely repulsive ($r_c = 2^{1/6}$), and τ_0 is negative. Including the attractive tail of the potential and increasing ε_w increases τ_0 to positive values, but the maximum value of τ_0 that we have found for incommensurate surfaces is $\sim 0.3\varepsilon/\sigma^3$ or 12 MPa. This value is comparable to the largest value observed between mica surfaces and also to the maximum pressures accessible in these experiments (12, 13). The pressures in typical load-bearing contacts are much larger. In this limit, τ_0 becomes irrelevant and μ_s approaches α.

Because experiments find different μ_s for different materials, some potential parameters must change α. Figure 2B shows the effect of changing one parameter at a time from our standard set. Increasing $\varepsilon_w/\varepsilon$ from 1 to 2 produces almost no change in τ_s, but decreasing σ_w/σ from 1.0 to 0.9 increases α by 50%, and increasing this ratio to 1.5 decreases α by a factor of 6. The opposite trend is seen for d/σ, where an increase from 1.2 to 1.5 increases α to 0.073.

These trends can be understood in terms of a simple geometrical model. At the large pressures of interest, the repulsive interactions between wall atoms and monomers are dominant. Atoms and monomers cannot be closer than an effective hard sphere diameter on the order of σ_w. This diameter is very insensitive to pressure because the repulsive force rises as $\varepsilon_w(\sigma_w/r)^{13}$ as r decreases. For the same reason, changing ε_w by a factor of 2 has little effect on the system. In contrast, decreasing σ_w/d allows monomers to penetrate more deeply into the wells between wall atoms. In order to slide, monomers must move up a ramp defined by the surface of closest approach. To overcome the normal load, F_s must equal L times the maximum slope of the ramps. As σ_w/d decreases, the ramps become steeper, resulting in the increase in α seen in Fig. 2B. We have confirmed that the surfaces do indeed move apart as the yield stress is approached and that this displacement increases with α.

The values of α in Fig. 2 range from 0.008 to 0.15 and are similar to measured values for some very smooth, weakly interacting surfaces such as MoS$_2$ (11) or mica (12). Most unlubricated macroscopic objects exhibit μ_s of 0.1 to 0.5 and have much more complex geometries, chemistries, and third bodies. It remains to be seen how our results relate to this rich spectrum of experimental systems. One possibility is that the atomic-scale roughness present on most surfaces increases α (16). For example, we find $\alpha = 0.3$ at a coverage of 1/8 for surfaces made by slicing through an amorphous solid. The inclusion of grain boundaries, steps, and other defects would also affect α. Some of the in-

crease in μ_s may be due to τ_0/P in Eq. 2. A final possibility is that more realistic models for hydrocarbon molecules and their interactions with surfaces would increase α. Some thin molecular layers are used as boundary lubricants to lower static friction, and the relation between molecular structure and the friction between incommensurate surfaces will be an interesting question for future studies.

References and Notes

1. D. Dowson, History of Tribology (Longman, New York, 1979).
2. F. P. Bowden and D. Tabor, The Friction and Lubrication of Solids (Oxford Univ. Press, Oxford, 1958).
3. G. M. McClelland and J. N. Glosli, in Fundamentals of Friction, H. M. Pollock and I. L. Singer, Eds. (Springer-Verlag, Berlin, 1990), pp. 405–425; G. A. Tomlinson, Philos. Mag. 7, 905 (1929).
4. K. Shinjo and M. Hirano, Surf. Sci. 283, 473 (1993); Y. I. Frenkel and T. Kontorova, Zh. Eksp. Teor. Fiz. 8, 1340 (1938).
5. A. Volmer and T. Natterman, Z. Phys. B 104, 363 (1997).
6. M. O. Robbins and E. D. Smith, Langmuir 12, 4543 (1996).
7. J. H. Dieterich and B. D. Kilgore, Pure Appl. Geophys. 143, 283 (1994); Tectonophysics 256, 219 (1996).
8. P. Berthoud and T. Baumberger, Proc. R. Soc. London Ser. A 454, 1615 (1998).
9. J. A. Greenwood and J. B. P. Williamson, ibid. 295, 300 (1966).
10. B. J. Briscoe and D. J. Tabor, J. Adhes. 9, 145 (1978); B. J. Briscoe and D. C. B. Evans, Proc. R. Soc. London Ser. A 380, 389 (1982).
11. I. L. Singer, in Fundamentals of Friction, I. L. Singer and H. M. Pollock, Eds. (Elsevier, Amsterdam, 1992), pp. 237–261.
12. M. L. Gee, P. M. McGuiggan, J. N. Israelachvili, A. M. Homola, J. Chem. Phys. 93, 1895 (1990); A. M. Homola, J. N. Israelachvili, P. M. McGuiggan, M. L. Gee, Wear 136, 65 (1990).
13. J. V. Alsten and S. Granick, Langmuir 6, 876 (1990); A. L. Demirel and S. Granick, J. Chem. Phys. 109, 1 (1998).
14. J. N. Glosli and G. M. McClelland, Phys. Rev. Lett. 70, 1960 (1993).
15. The interfacial interactions may be strong enough to meet this condition in special cases, such as clean metal surfaces in ultrahigh vacuum.
16. Real surfaces are rarely perfect single crystals, but including disorder without third bodies does not seem to explain experimental observations. The static friction between stiff random surfaces is a finite-size effect that drops as the inverse of the contact diameter. We find that values can be appreciable on the scale of AFM tips (<40 atomic diameters), but not in micrometer-scale contacts. Elastic deformation at large scales can yield static friction, but the values are exponentially small for weak disorder (5).
17. J. Krim, D. H. Solina, R. Chiarello, Phys. Rev. Lett. 66, 181 (1991); C. Mak and J. Krim, Phys. Rev. B 58, 5157 (1998).
18. M. Cieplak, E. D. Smith, M. O. Robbins, Science 265, 1209 (1994); M. S. Tomassone, J. B. Sokoloff, A. Widom, J. Krim, Phys. Rev. Lett. 79, 4798 (1997); B. N. J. Persson and A. Nitzan, Surf. Sci. 367, 261 (1996).
19. M. Hirano, K. Shinjo, R. Kaneko, Y. Murata, Phys. Rev. Lett. 78, 1448 (1997).
20. J. x. Martin, Phys. Rev. B 48, 10583 (1993).
21. M. Schoen, C. L. Rhykerd Jr., D. J. Diestler, J. H. Cushman, Science 245, 1223 (1989).
22. P. A. Thompson and M. O. Robbins, ibid. 250, 792 (1990).
23. ———, G. S. Grest, Isr. J. Chem. 35, 93 (1995); E. Manias, G. Hadziiaoannou, G. ten Brinke, J. Chem. Phys. 101, 1721 (1994).
24. M. D. Perry and J. A. Harrison, J. Phys. Chem. B 101, 1364 (1997); Thin Solid Films 290, 211 (1996).
25. J. P. Gao, W. D. Luedtke, U. Landman, Phys. Rev. Lett. 79, 705 (1997).
26. K. Kremer and G. S. Grest, J. Chem. Phys. 92, 5057 (1990).
27. Financial support from NSF grant DMR-9634131 is gratefully acknowledged. We are also grateful to Intel for donating workstations on which these simulations were run.

16 February 1999; accepted 21 April 1999

Experimental Evidence for the Source of Excess Sulfur in Explosive Volcanic Eruptions

Hans Keppler

The amounts of sulfur released in explosive volcanic eruptions are often orders of magnitude larger than those expected to result from the degassing of the erupted SiO$_2$-rich magma. Experimentally measured fluid/melt partition coefficients of sulfur ranged from 47 under oxidizing conditions (where SO$_2$ is the dominant sulfur species in the fluid) to 468 under reducing conditions (where H$_2$S dominates). Therefore, a few weight percent of hydrous fluid accumulated in the top of a magma chamber may extract most of the sulfur out of the entire magma reservoir and generate sulfur excesses upon eruption.

Explosive volcanic eruptions often inject enormous amounts of sulfur dioxide into the stratosphere (1–8). Oxidation of SO$_2$ produces sulfate aerosols that can backscatter sunlight for months or even years after the erup-

Bayerisches Geoinstitut, Universität Bayreuth, 95440 Bayreuth, Germany.

tion (9). Accordingly, it is believed that the release of sulfur is mainly responsible for the subsequent global cooling observed after explosive volcanic activity (9–13). Amounts of volcanic sulfur measured from satellites are often orders of magnitude larger than those expected to result from the degassing of the erupted silicic melt. The 1991 eruption of